DOI 10.5162/Ultrasonic2025/A2-b5



# Enhancing Air Purification: Ultrasound-Based Filtration of Ultrafine Aerosols and Gaseous Pollutants

*Patrick Haas*[1], *Sabrina Tietze*[1], *and Klaus Stefan Drese*[1]
[1] *Institute of Sensor and Actuator Technology (ISAT), University of Applied Sciences Coburg, Am Hofbräuhaus 1b, 96450 Coburg, Germany*
*patrick.haas@hs-coburg.de*

**Abstract:** Since COVID-19, clean indoor air has become more of a focus due to airborne viruses. Conventional filters often fail to capture ultrafine particles. This work investigates how standing ultrasonic fields manipulate aerosols for more efficient cleaning. Gor'kov theory and FEM simulations used to evaluate the acoustic forces on particles. Experiments by light refractive vibrometry and high-speed camera observations confirm the model quality.

**Keywords:** Acoustic manipulation, Gor'kov potential, FEM simulation, air purification, levitation

## Introduction

Since the COVID-19 pandemic, the importance of clean indoor air has gained renewed attention due to airborne transmission of viruses and aerosols. Conventional air purifiers often struggle to effectively capture ultrafine particles and gaseous pollutants. In this work, we explore the use of ultrasound not merely for filtration enhancement, but specifically to manipulate aerosol particles within an airstream. By generating standing acoustic waves, particles can be influenced and concentrated at defined positions, enabling novel approaches to air purification. In the first step, the study investigates the behavior of particles in acoustic fields based on the analytical Gor'kov model and finite element simulations (FEM). Theoretical investigations are compared with experiments. Our aim is to demonstrate how acoustic forces can be used to actively control aerosol distribution in airflows and thus create the basis for advanced cleaning technologies.

## Methods and Calucations

To set the parameters for the calculations in a first step, a wind tunnel including an acoustic resonator chamber was designed. The top of the wind tunnel of Fig. 1 consisted of an inlet (1), a flow straightener (2), the acoustic resonator chamber (4) with connecting pieces (3) and the fan (5), which drew in the air. With the wind tunnel, it was possible to generate disturbance velocities from 0 $\frac{\mathrm{m}}{\mathrm{s}}$ to 9 $\frac{\mathrm{m}}{\mathrm{s}}$.
The resonator chamber has been designed so that the interior of the resonator can be observed using a camera (VW 600C, Keyence Deutschland GmbH, Frankfurt am Main, Germany) and a vibrometer (PSV 400M, Polytec GmbH, Waldbronn, Germany).

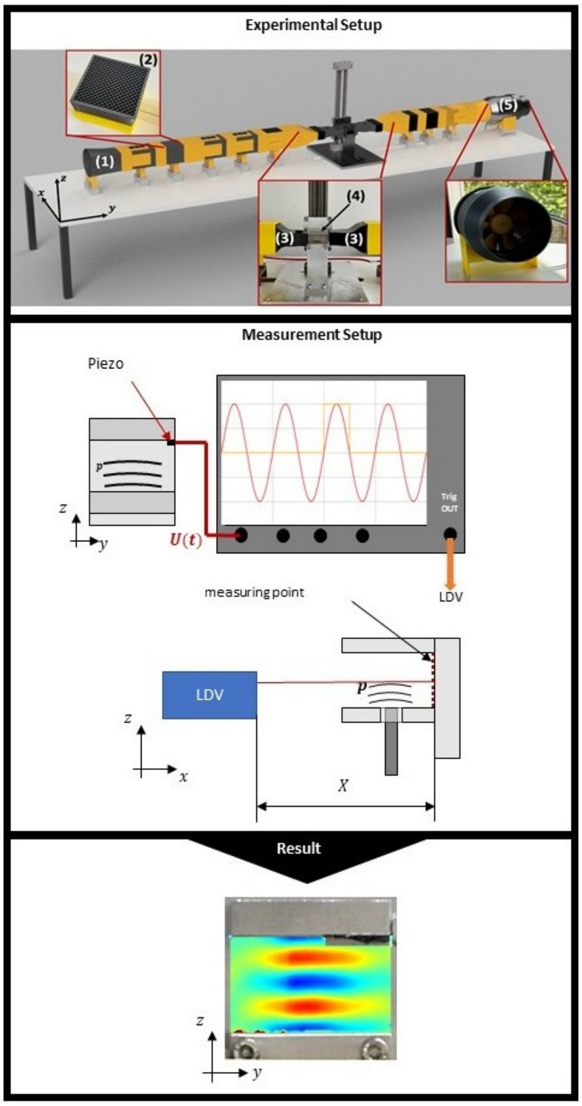


*Fig. 1: Measurement setup for measuring the pressure fields in the resonator chamber with the Laser Doppler Vibrometer.*

In addition, there is an external recess in the base of the resonator chamber to accommodate the ultrasonic horn (UP200S, Hielscher Ultrasonics GmbH, Teltow, Germany). The ultrasonic horn in conjunction with a reflector of steel on the opposite side of the wind tunnel is used to generate the standing wave field. The following considerations were made to determine the optimum distance between the reflector and the ultrasonic horn.
For the theoretical predictions, the analytical model of Gor'kov [1] is compared with FEM done by COMSOL Multiphysics version 6.1. For resonance to occur, the distance between the ultrasonic horn and the reflector $l_z$ must be an integer multiple of half the wavelength of the acoustic wave $\lambda$. The wave number $k$ for the direction are defined as [1]–[3]:

$$k = \frac{n\pi}{l_z}, n \in \mathbb{N} \tag{1}$$

The sound potential $U$, from which the acoustic pressure and velocity can be derived, is defined in the three spatial directions x, y, z as:

$$U(x, y, z, t) = \frac{\hat{\xi}\omega}{|\vec{k}|} \cos\left(\frac{n_x \pi}{l_x} x\right) \cos\left(\frac{n_y \pi}{l_y} y\right) \cos\left(\frac{2\pi}{\lambda} z\right) \sin(\omega t) \tag{2}$$

Whereas $\omega$ is the angular frequency. The acoustic velocity and pressure are then obtained by:

$$\vec{v} = \nabla U, \quad p = -\rho \frac{\partial U}{\partial t} \tag{3}$$

For small spherical particles $R \ll \lambda$, the time-averaged acoustic radiation force can be derived from the Gor'kov potential $U_{rad}$, given by [1], [4], [5]:

$$U_{rad} = \frac{4\pi}{3} R^3 \left[\frac{f_1}{2\kappa_{\mathrm{air}}} \langle p^2 \rangle - \frac{3 f_2}{4 \rho_{\mathrm{air}}} \langle v^2 \rangle \right] \tag{4}$$

The contrast factors $f_1$ and $f_2$ depend on the material properties of the particle and the surrounding medium:

$$f_1 = 1 - \frac{\kappa_{\mathrm{p}}}{\kappa_{\mathrm{air}}}, \quad f_2 = \frac{2\left(\rho_{\mathrm{p}/\rho_{\mathrm{air}}-1}\right)}{2\rho_{\mathrm{p}/\rho_{\mathrm{air}}+1}} \tag{5}$$

Here $R$ is the radius of the particle and the coefficients $f_1$ and $f_2$ are dimensionless coefficients that take into account the properties of the material (density $\rho$ and compression modulus $\kappa$) of the particle (index *p*) and the surrounding medium (index *air*). The brackets $\langle\cdot\rangle$ in Eq. (4) indicate time averages. The first term in Eq. (4) $f_1/2 \cdot \kappa_{\mathrm{air}} \langle p^2 \rangle$ describes the effect of the pressure field on the drop, while the second term $3f_2/4\rho_{\mathrm{air}} \langle v^2 \rangle$ describes the dynamic effects due to the movement of the medium. The acoustic radiation force is then given by the gradient of the Gor'kov potential:

$$\vec{F}_{rad} = -\nabla U_{rad} \tag{6}$$

For larger particles, the acoustic force can be calculated as [6], [7]:

$$\vec{F}_{rad} = -\oint_{\partial\Omega_0} \left[\left(\frac{\rho\langle v^2\rangle}{2} - \frac{\langle p^2 \rangle}{2\rho c^2}\right)\vec{n} - \rho\langle(\vec{n}\cdot\vec{v})\vec{v}\rangle\right] dA. \tag{7}$$

For the force in the z-direction, the force contribution $F_z$ is considered in more detail. Furthermore, the spatial coordinates in the x- and y-directions are set to zero $F_z{}^{\mathrm{rad}}(0, 0, z) = F_z$. This writes the force in the z-direction [8]:

$$F_z = \underbrace{-\pi R^3 \left(-\frac{1}{3} f_1 \kappa_{\mathrm{air}} p^2_{\mathrm{max}} - \frac{1}{2} f_2 v^2_{\mathrm{max}} \rho_{\mathrm{air}} \frac{k_z^3}{k^2}\right)}_{F_{\mathrm{z,\ max}}=\mathrm{const.}} \cdot \sin(2k_z z) \tag{8}$$

If one investigates Eq. (8), one can see that the force field in the z-direction has twice the frequency of the original pressure field [9]. Another statement can be derived from Eq. (8). The force curve shows that the acoustic force direction changes every $\lambda/4$. As a result, the acoustic force points sometimes in and sometimes against the weight force, which means that particles cannot form and accumulate in every area of the pressure field. Particles can only accumulate where the weight force is balanced by the acoustic force.
To verify theoretical predictions without air flow, standing wave fields are visualized using the refractive vibrometry method [10] and nodes are visualized using levitated droplets and a camera.

**Results**

To validate the FEM, the pressure field between the ultrasonic horn and the resonator plate is first simulated at various distances, including distances outside the resonance condition. In addition, the pressure field is determined experimentally using the light refractive vibrometry method. The results can be found in Fig. 2. As this is a qualitative comparison of the pressure fields, no colour bar has been used. The pressure free areas are shown in green. As can be seen, a standing wave field is formed for the distances $l_z = \lambda$ and $l_z = 2\lambda$ (Fig. 2 third and fourth lines), because of the pressure bulges or pressure troughs. At a distance of $l_z = 8\,\mathrm{mm}$ (Fig. 2 first line) an asymmetric spatial mode seems to form. At a distance of $l_z = 12\,\mathrm{mm}$ (Fig. 2 second line) a weak pressure bulge appears in the center. However, due to the distance $l_z = N \times \frac{\lambda}{2}$, the condition of a standing wave is not yet fulfilled, i.e. the pressure field has no pressure bulges or pressure troughs and nodes. The pressure fields of the experiments are in good agreement with the predicted pressure fields by FEM.

DOI 10.5162/Ultrasonic2025/A2-b5

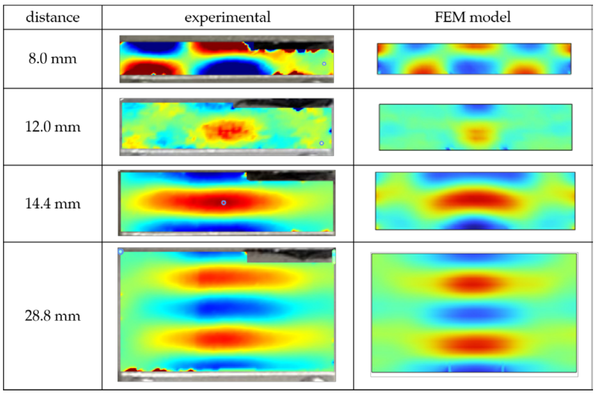


*Fig. 2: Qualitative representation of the pressure fields at different distances left from the experiment, right from FEM model at various distances of the resonator plates. The missing measurement window in the right-hand corner of each experimental measurement was removed from the measurement because the trigger piezo was attached at this point and therefore no measurement was possible at these points.*

A closer look at the pressure fields predicted by the analytical model and the FEM reveals a high degree of similarity when compared with the experiments for a resonator length of $l_z = \lambda$ or $l_z = 2\,\lambda$. Similar values were found for the z-coordinates of the pressure bellies and nodal points of the standing compression spring. The compared values can be seen in Tab. 1.
Last particles in the form of water droplets are introduced into the resonator. The arrangement of the water droplets in the resonator can be seen at the level of the nodal points if the FEM data is placed next to them, see Fig. 3.

*Tab. 1: Calculated node and extrema positions (in $\lambda$) for different models and resonator lengths $l_z$.*

| **Model** | **z positions (in $\lambda$)** |
|---|---|
| FEM $l_z$=$\lambda$ | **Nodes:** 0.232, 0.751 |
| | **Extrema:** 0.492 |
| Analytical $l_z$=$\lambda$ | **Nodes:** 0.25, 0.75 |
| | **Extrema:** 0.5 |
| LDV $l_z$=$\lambda$ | **Nodes:** 0.24, 0.79 |
| | **Extrema:** 0.52 |
| FEM $l_z$=$2\lambda$ | **Nodes:** 0.254, 0.737, 1.24, 1.76 |
| | **Extrema:** 0.496, 0.987, 1.50 |
| Analytical $l_z$=$2\lambda$ | **Nodes:** 0.25, 0.75, 1.25, 1.75 |
| | **Extrema:** 0.5, 1.0, 1.5 |
| LDV $l_z$=$2\lambda$ | **Nodes:** 0.25, 0.75, 1.25, 1.76 |
| | **Extrema:** 0.5, 1.0, 1.51 |

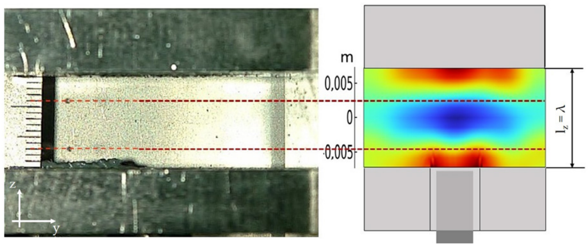


*Fig. 3: Levitated droplets in their stability points (left) compared with the FEM pressure field $l_z = \lambda$ (right).*

### Discussion

When analyzing the two-dimensional pressure fields in Fig. 2 and comparing the LDV measurements with the FEM, a good qualitative agreement between the LDV measurements and the FEM simulation can be observed. For the distance of 8 mm in Fig. 2, there is a slight deviation between the FEM and the LDV measurement. This deviation is due to the limitation of the calculation space in the FEM model, which does not prevail in the measurement.
The deviations in the position of the zero points (nodes) and the extreme values (bellies) between the theoretical pressure fields and the simulations listed in Tab. 1 occur at all distances considered ($l_z = \lambda$ and $l_z = 2\lambda$ ). The pressure field from the analytical model assumes that the propagating waves are excited by the entire width of the lower resonator plate and thus have flat wave fronts over the entire width and interfere from a standing wave in the resonator.

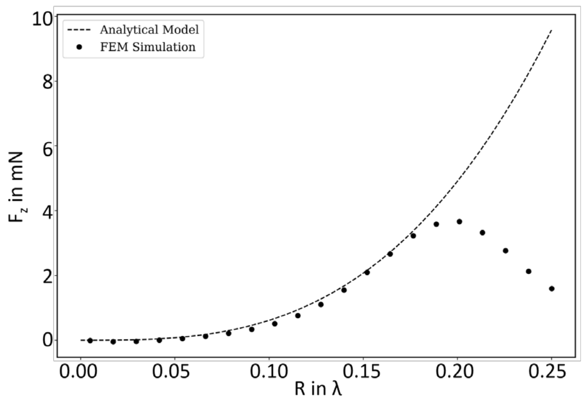


*Fig. 4: The force curves as a function of the radius of the droplet are shown for each of the models. The force resulting from the Gor'kov potential is shown as a dashed line, with the dots representing the forces resulting from the FEM model. Both forces curves were evaluated at the point ($x = 0$ m, $y = 0$ m, $z = \frac{5\lambda}{8}$).*

DOI 10.5162/Ultrasonic2025/A2-b5

In the pressure fields from the FEM and the pressure fields from the LDV measurement, the pressure field is excited by the tip of the ultrasonic horn with a limited diameter of 14 mm, which causes waves with curved wave fronts to propagate and thus waves with curved wave fronts to intefere into a standing wave field. This can be a cause that leads to the differences in the model. Fig. 3 shows that the droplets accumulate in the nodal points. However, a further estimation between the Gor'kov model and the FEM (Fig. 4) shows that with increasing particle size, an estimation using Gor'kov is no longer possible to determine the force influence on the droplets.

### Conclusion

The aim of this work was to achieve acoustic air purification. For this purpose, a test rig was constructed, the dimensions of which were then used to set up analytical models, FEM and experiments to verify the theoretical models. It was shown that the theoretical pressure field can also be verified using light refractive methods, which confirms the theory. It was also possible to observe the influence of droplets using a camera. Furthermore, it was shown that Gorkov's model can be used for the design of small particles or droplets, while FEM must be used for larger particles. The next step will be to set up several or longer resonators based on these results and generate an air flow charged with water dropletes in the test set-up.

### Acknowledgement

The authors would like to thank the team of the Institute of Sensor and Actuator Technology especially Siegfried Vorister for his expertise in constructing the resonator and for his technical guidance throughout the design of the test rig. The support of this research by 'Technologieallianz Oberfranken (TAO)' is gratefully acknowledged. The work was financial supported by the Alfred Kärcher Foundation.

### References

[1] L. Gor'Kov, 'On the forces acting on a small particle in an acoustical field in an ideal fluid,' *Soviet Physics Doklady*, vol. 6, pp. 773–775, 1962.

[2] S. Weinzierl, *Handbuch der Audiotechnik*. Berlin, Germany: Springer Science & Business Media, 2008.

[3] M. Dewar, 'Einführung in die moderne chemie: Lehrbuch für naturwissenschaftler und mediziner in den anfangssemestern,' in *Einführung in die moderne Chemie*, Berlin, Germany: Springer Berlin Heidelberg, 1970, pp. 57–70.

[4] L. Worstmann, 'Stability of a particle levitated in an acoustic field,' *Acoustic Levitation*, vol. 5, 2016.

[5] G. Simon, M. Andrade, M. Desmulliez, M. Riehle and A. Bernassau, 'Numerical determination of the secondary acoustic radiation force on a small sphere in a plane standing wave field,' *Micromachines*, vol. 10, p. 431, 2019, 10.3390/mi10070431.

[6] M. Barmatz and P. Collas, 'Acoustic radiation potential on a sphere in plane, cylindrical, and spherical standing wave fields,' *Journal of the Acoustical Society of America*, vol. 77, pp. 928–945, 1985, 10.1121/1.392061.

[7] H. Bruus, 'Acoustofluidics 7: The acoustic radiation force on small particles,' *Lab on a Chip*, vol. 12, pp. 1014–1021, 2012, 10.1039/C2LC21068A.

[8] C. Devendran, D. R. Billson, D. A. Hutchins and A. Neild, 'Optimisation of an acoustic resonator for paricles manipulation in air,' *Sensors and Actuators B: Chemical*, vol. 224, pp. 529–538, 2016, 10.1016/j.snb.2015.10.068.

[9] L. V. King, 'On the acoustic radiation pressure on spheres,' *Proc. R. Soc. Lond. A*, vol. 147 (861), pp. 212–240, 1934, 10.1098/rspa.1934.0215.

[10] S. Tietze and G. Lindner, 'Visualization of the interaction of guided acoustic waves with water by light refractive vibrometry,' *Ultrasonics*, vol. 99, p. 105 995, 2019, 10.1016/j.ultras.2019.105955.